Advance Publication

IEEJ Journal of Industry Applications
J-STAGE Advance published date : Feb. 17, 2023
DOI : 10.1541/ieejjia.22010162

Paper

Feedback Error Learning-Based Position Control in Position-Sensorless Positioning Servo Systems for IPMSMs

Naoki Kawamura[*,**] Member, Shota Inoue[***] Non-member
Tadanao Zanma[***] Senior Member, Keiichiro Kondo[**] Senior Member
Kenta Koiwa[***] Member, Kang-Zhi Liu[***] Member
Masaaki Shibata[*] Senior Member

Position-sensorless positioning servo systems for interior permanent magnet synchronous motors (IPMSMs) have been developed to achieve dimension and cost reduction. In these systems, parameter mismatch between the IPMSM, position controller, and position estimator due to thermal variation and aged deterioration is inevitable. To solve this problem, a parameter identification method based on an adaptive scheme has been proposed. However, to use the adaptive scheme, this method can only be applied under no-load conditions, and it is difficult to compensate for parameter variations during actual operation, i.e., under load conditions.

This paper proposes a novel learning-based position control in position-sensorless positioning servo systems. In the proposed method, a feedfoward controller established via learning adaptively compensates the parameter fluctuations in these systems. As learning progresses, the transient response of position control is improved while ensuring robustness to disturbance torque. The effectiveness of the proposed position control system is demonstrated via experiments.

Keywords: Position-sensorless control, Positioning servo system, Learning control, Feedback error learning, and IPMSM.

1. Introduction

Positioning servo systems of interior permanent magnet synchronous motors (IPMSMs) with position sensors such as encoders have been widely used in many industrial applications. Since the sensor increases cost and dimension, position-sensorless positioning servo systems have been developed [(1)~(5)]. There exist two well-known methods of position estimation: one using the saliency of IPMSMs [(1)(2)] and the other using the high-frequency voltage injection [(3)(4)]. Motor design to improve position estimation has also been discussed [(5)].

The position-sensorless positioning servo systems require high-accurate and high-speed position control. In most cases, the servo systems are designed using the parameters of IPMSMs. The parameters fluctuate according to environmental changes and/or load changes, which results in performance deterioration of position control. Nevertheless, the controller design itself or the parameters fluctuation has not been discussed sufficiently in literature. The ideal position controller is given by the inverse system of the IPMSM model. Therefore, it is necessary to obtain the parameters of IPMSMs to achieve high-performance positioning control.

We proposed a dynamic certainty equivalence (DyCE) adaptive scheme to estimate the parameters of IPMSM [(6)(7)]. We also showed that the parameters of IPMSM were successfully estimated by the proposed method even if they fluctuated with temperature and environmental changes. Although the parameter estimation is stabilized, the estimated parameters are needed to be differentiated for the input to the automatic current regulator (ACR) [(7)]. If the load changes abruptly, the estimated parameters also change accordingly. In this case, the input to the ACR becomes excessive due to the derivative of the estimated parameters. In general, a limiter, such as a saturator, is inserted in the control loop. This limiter makes the system nonlinear. As a result, the stability of the parameter estimation by the adaptive scheme is no longer guaranteed. The parameters are estimated so that the control error is zero [(7)]. If the control error is suppressed so fast by a high-gain FB controller, the parameters are not successfully estimated. In addition, a high-gain feedback controller is susceptible to observation noise. Thus, it is difficult to increase the gain of the FB controller.

We focus on a feedback-error learning (FEL) control [(8)~(11)] to overcome the instability of parameters estimation. The FEL controller consists of one feedfor-

[*] Faculty of Science and Technology, Seikei University
3–3–1, Kichijoji-Kitamachi, Musashino, Tokyo, 180–8633 Japan
[**] School of Advance Science and Engineering, Waseda University
3–4–1, Okubo, Shinjuku, Tokyo, 169–8555 Japan
[***] Graduate School of Engineering, Chiba University
1–33, Yayoi, Inage, Chiba, 263–8522 Japan

© 2022 The Institute of Electrical Engineers of Japan.

Table 1. Notation.

i_d, i_q	d- and q-axis currents
v_d, v_q	d- and q-axis voltages
L_d, L_q	d- and q-axis stator inductances
ψ_f	electromotive force constant
R	stator winding resistance
P	number of pole pairs
ω_{re}	electric angular velocity of rotor
θ_{re}	electric angle of rotor
J_n	inertia

ward (FF) and one FB controllers. The FF controller is trained to reduce the output from the FB controller, i.e., the FF controller learns the inverse system of the controlled plant. As a result, transient response is improved.

This paper proposes a novel FEL-based position control system in the position-sensorless positioning servo systems. In the proposed method, the FF controller established via learning compensates the parameter fluctuations adaptively in the systems. In the proposed position control system, a phase delay compensator is arranged parallel to the controlled plant for stabilizing the learning under no load. The phase delay compensator can also avoid the differential operation of the estimated parameters. Thus, an excessive input to the ACR can be avoided even the load changes. As a result, the stability of learning can be ensured regardless of load.

As the learning progresses, the output of the FEL controller becomes dominant than the FB controller. Thus, the transient response of the position control is improved. Since the FB controller continues to operate even after completion of the learning, robustness to the disturbance torque is guaranteed. The effectiveness of the proposed position control system is shown through experiments.

This paper is organized as follows: Section 2 reviews the conventional position-sensorless positioning servo system (7) and describes the issues in the position control system. In Section 3, we propose an FEL-based position control system. Section 4 demonstrates the effectiveness of the proposed position control system via experiments. Section 5 concludes this paper.

Table 1 lists the notations used in this paper. In this paper, for a variable or a signal x, $\hat{x}$ and x^* denote the estimation and the reference of x, respectively. For a function of time x, $\dot{x}$ denotes $\frac{\mathrm{d}}{\mathrm{d}t}x$.

2. System Configuration

Fig. 1 shows the configuration of the position-sensorless positioning servo system addressed in this paper. In Fig. 1, the subscript "uvw" attached to $\boldsymbol{v}$ and $\boldsymbol{i}$ indicates "three-phase" and the superscript "$*$" attached to a symbol is its reference. The system shown in Fig. 1 consists of the PI-type ACR, comb-filter-based position estimator, controlled plant, and position control system.

The role of the position controller is to generate the current reference to the ACR. Since the performance of position estimation under load was verified in (12), we assume that 1) the ACR functions well, i.e., $i_q \approx i_q^*$, and 2) the position estimator also functions well, i.e., $\hat{\theta}_{\mathrm{re}} \approx \theta_{\mathrm{re}}$, and thus, $i_\delta \approx i_q$. The validity of these assumptions has been demonstrated (7). By these assumptions, we can redraw Fig. 1(a) as (b) focusing on the position controller. Hereafter, we limit ourselves to the position controller (see (7) (12) for the details of the structure of the comb-filter-based position estimator).

The transfer function from i_q^* to θ_{re} in Fig. 1 is denoted by $s^{-1}P(s)$, and is given by the following third-order system:

$$s^{-1}P(s) = \frac{1}{s(\alpha_2 s^2 + \alpha_1 s + \alpha_0)}, \tag{1}$$

where α_i $(i = 1, 2, 3)$ includes the parameters such as R, L_q, ψ_f and J_n, which varies with environmental and/or load change.

2.1 Conventional position control system (7) Fig. 2 shows the configuration of the positioning controller of the conventional method (7). The positioning controller is composed of an adaptive scheme and a PD-type automatic position regulator (APR).

From (1), the ideal FF compensator is given by $P^{-1}(s)s$, and thus, the ideal input to the ACR denoted by u_0 is given by

$$\begin{aligned} u_0 &= P^{-1}(s)s\theta_{\mathrm{re}}^* \\ &= \boldsymbol{\alpha}^\top \dot{\boldsymbol{\xi}}, \end{aligned} \tag{2}$$

where $\boldsymbol{\alpha} = \begin{bmatrix}\alpha_2 & \alpha_1 & \alpha_0\end{bmatrix}^\top$ and $\boldsymbol{\xi} = \begin{bmatrix}\ddot{\theta}_{\mathrm{re}}^* & \dot{\theta}_{\mathrm{re}}^* & \theta_{\mathrm{re}}^*\end{bmatrix}^\top$. Ideally, if u_0 in (2) is input to the ACR, then $u_{\mathrm{FB}} = 0$.

Since $\boldsymbol{\alpha}$ in (2) is variable due to the parameter fluctuations, we estimate it as $\hat{\boldsymbol{\alpha}}$. Replacing $\boldsymbol{\alpha}$, $P(s)$, and u_0 in (2) with $\hat{\boldsymbol{\alpha}}$, the estimated $\hat{P}(s)$, and u_{FF}, respectively, we consider

$$\begin{aligned} u_{\mathrm{FF}} &= \hat{P}^{-1}(s)s\theta_{\mathrm{re}}^* \\ &= \hat{\boldsymbol{\alpha}}^\top \dot{\boldsymbol{\xi}} \\ &= C(s)\left(\hat{\boldsymbol{\alpha}}^\top\left(\frac{1}{C(s)}\dot{\boldsymbol{\xi}}\right)\right), \end{aligned} \tag{3}$$

where $C(s)$ is an additional polynomial. The stability of $\hat{\boldsymbol{\alpha}}$ in (3) was solved by a phase-lead compensator $C(s)$ in series with $\hat{P}^{-1}(s)s$ as shown in Fig. 2 such that the passivity (13) (14) was satisfied (7).

For convenience, we define

$$e := \theta_{\mathrm{re}}^* - \theta_{\mathrm{re}}. \tag{4}$$

When $C(s) = s(Ks + 1)$ $(K > 0)$, the behavior of $\hat{\boldsymbol{\alpha}}$ is given by

$$\begin{aligned} \dot{\hat{\boldsymbol{\alpha}}} &= \Gamma\left(\frac{\dot{\boldsymbol{\xi}}}{C(s)}e\right) \\ &= \Gamma\left(\frac{\dot{\boldsymbol{\xi}}}{s(Ks+1)}e\right) \\ &= \Gamma\left(\frac{\boldsymbol{\xi}}{Ks+1}e\right), \end{aligned} \tag{5}$$

where Γ is an adaptive gain matrix.

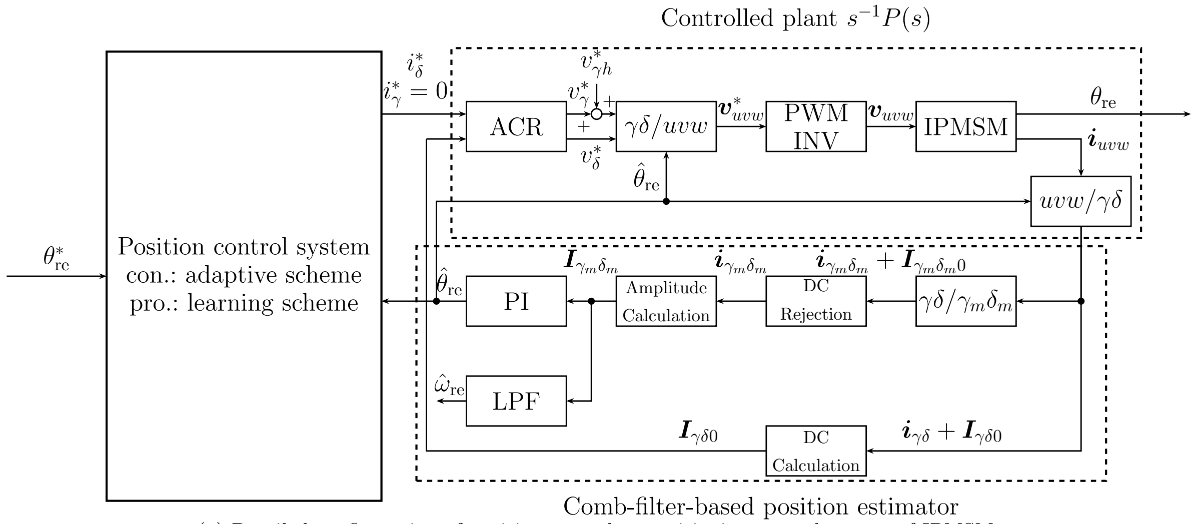

(a) Detailed configuration of position-sensorless positioning control system of IPMSM.

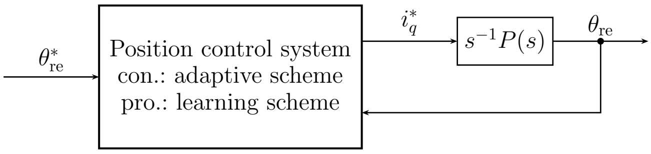

(b) Equivalent configuration focusing on position control system.

Fig. 1. Configuration of position-sensorless positioning control system of IPMSM.

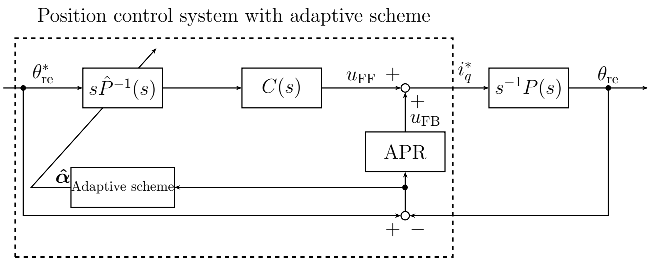

Fig. 2. Conventional position control system [7].

In addition, applying the swapping lemma [15] to (3), we recast (3) as

$$\begin{aligned} u_{\mathrm{FF}} &= C(s)\left(\hat{\boldsymbol{\alpha}}^\top\left(\frac{1}{C(s)}\dot{\boldsymbol{\xi}}\right)\right) \\ &= K\ddot{\hat{\boldsymbol{\alpha}}}^\top\frac{1}{Ks+1}\boldsymbol{\xi} + \dot{\hat{\boldsymbol{\alpha}}}^\top\left(2\boldsymbol{\xi} - \frac{1}{Ks+1}\boldsymbol{\xi}\right) + \hat{\boldsymbol{\alpha}}^\top\dot{\boldsymbol{\xi}}. \end{aligned} \tag{6}$$

In (6), $\ddot{\hat{\boldsymbol{\alpha}}}$ is obtained by differentiating $\dot{\hat{\boldsymbol{\alpha}}}$ in (5). If $\ddot{\hat{\boldsymbol{\alpha}}}$ in (6) is large, u_{FF} becomes excessive. Inserting a limit such as a saturator to prevent such an excessive input makes the system nonlinear. Since the adaptive scheme is supposed to work in linear systems, the stability of $\hat{\boldsymbol{\alpha}}$ in (5) is no longer guaranteed due to the nonlinearity.

The APR has another issue. If the APR is high-gain to improve disturbance suppression performance, then e in (4) becomes small relatively fast. In this case, $\dot{\hat{\boldsymbol{\alpha}}}$ in (5) also becomes small, which decreases the estimation speed of $\hat{\boldsymbol{\alpha}}$. In other words, there exists a trade-off between the disturbance suppression performance and the convergence speed of $\hat{\boldsymbol{\alpha}}$. This trade-off results in insufficient pole-zero cancellation between $\hat{P}^{-1}(s)s$ and $s^{-1}P(s)$ immediately after a load is applied, which reduces the phase margin. Therefore, the gain of the APR must be small, which sacrifices the disturbance suppression performance.

To summarize the above discussion, there exist the following issues to be solved in the conventional method [7]:

- instability of behavior of $\hat{\boldsymbol{\alpha}}$ due to the nonlinearity of the limit to prevent the excessive inputs to the ACR and
- the trade-off between disturbance suppression performance and estimation speed of $\hat{\boldsymbol{\alpha}}$ for the gain of APR.

3. Proposed position control system

To overcome the two issues described at the end of the previous section, we propose an FEL-based position control system. As in the previous section, we assume that $\hat{\theta}_{\mathrm{re}} \approx \theta_{\mathrm{re}}$, and thus, $i_\delta \approx i_q$. Fig. 3 shows the proposed position control system. As shown in Fig. 3, the phase-lead compensator $C(s)$ is arranged in parallel to $s^{-1}P(s)$ instead of a serial connection to it. This arrangement avoids differential computation of $\ddot{\hat{\boldsymbol{\alpha}}}$, which prevents excessive input to the ACR. This method is called a parallel feedforward compensator (PFC), which is well-known as the FB controller design method to satisfy the passivity of the closed-loop system [16]. The proposed FEL system estimates u_{FF}, i.e., the ideal q-axis current reference such that θ_{re} agrees with θ^*_{re}, instead of $\hat{\boldsymbol{\alpha}}$. Although a high-gain APR suppresses e in (4), learning speed of u_{FF} becomes slow due to small e if e is used as the training data in the FEL. By contrast, if u_{FB} is used instead of e as as the training data in the FEL, learning of u_{FF} is accelerated by rich u_{FB} which is

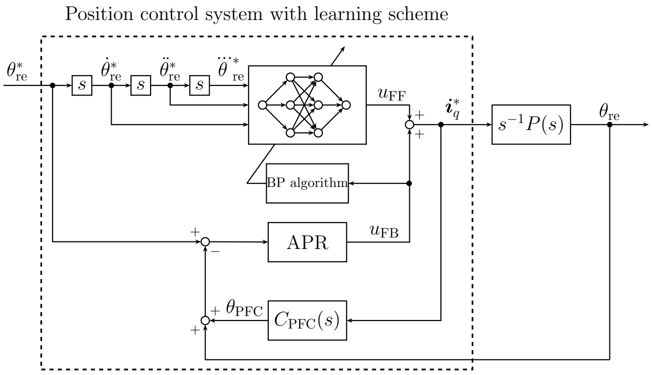

Fig. 3. Proposed position control system.

the output of high-gain APR. Thus, the FEL solves the trade-off between disturbance suppression performance and learning speed of $u_{\rm FF}$ by using $u_{\rm FB}$ as the training data. However, a saturator that limits excessive $u_{\rm FB}$ due to the high-gain APR causes nonlinearity of $u_{\rm FB}$. The nonlinearity of $u_{\rm FB}$ hinders learning of $u_{\rm FF}$ in the conventional methods described in Section 2 in which the linearity of $u_{\rm FB}$ is assumed. This brings another issue in the FEL.

To solve the issue, we adopt the NN with more than two layers since $u_{\rm FF}$ can be learned even if $u_{\rm FB}$ is nonlinear by the NN.

3.1 PFC The PFC stabilizes the learning of $\hat{P}^{-1}(s)s$ by designing $C_{\rm PFC}(s)$ such that the relative degree of the augmented transfer function $\tilde{G}(s) = s^{-1}P(s) + C_{\rm PFC}(s)$ from i^*_q to $(\theta_{\rm re} + \theta_{\rm PFC})$ becomes one for satisfying the passivity. In this paper, the APR is designed as a PD controller, which can be regarded as a first-order phase lead compensator. Since the relative degree of the open-loop transfer function composed of $s^{-1}P(s)$ and the APR is two, we can design $C_{\rm PFC}(s)$ as a first-order delay system such that the relative degree of $\tilde{G}(s) = \hat{P}^{-1}(s)s + C_{\rm PFC}(s)$ becomes two. Thus, we design $C_{\rm PFC}(s)$ as the following first-order delay system:

$$C_{\rm PFC}(s) = \frac{K\omega_c}{s+\omega_c}, \tag{7}$$

where ω_c and K are the cut-off frequency and the gain, respectively. In (7), ω_c should be sufficiently lower than the frequencies included in $\theta^*_{\rm re}$ while K is adjusted by confirming the response of $\hat{\theta}_{\rm re}$ and the steady-state value of $\theta_{\rm PFC}$. From (1) and (7), $\tilde{G}(s)$ is given as

$$\begin{aligned}\tilde{G}(s) &= s^{-1}P(s) + C_{\rm PFC}(s)\\ &= \frac{K\omega_c\alpha_2 s^3 + K\omega_c\alpha_1 s^2 + (K\omega_c\alpha_0 + 1)s + \omega_c}{\alpha_2 s^4 + (\alpha_1 + \omega_c\alpha_2)s^3 + (\alpha_0 + \omega_c\alpha_1)s^2 + \omega_c\alpha_0 s}.\end{aligned} \tag{8}$$

We consider $\tilde{G}(s)$ in (8) instead of $s^{-1}P(s)$ to stabilize the learning of $\hat{P}^{-1}(s)s$. Using (8) and the APR, we obtain the relationship between $u_{\rm FB}$ and $\hat{P}^{-1}(s)s - P^{-1}(s)s$ as

$$u_{\rm FB} = \underbrace{\frac{-\tilde{G}(s)(K_P + sK_D)}{1 + \tilde{G}(s)(K_P + sK_D)}}_{=:G_{\rm FEL}(s)}(\hat{P}^{-1}(s)s - P^{-1}(s)s)\theta^*_{\rm re}, \tag{9}$$

where K_P and K_D are determined by trial and error such that the step response of $\omega_{\rm re}$ is at the desired cut-off frequency (see Appendix for the detail). In (9), the relative degree of $G_{\rm FEL}(s)$ is zero, i.e., $G_{\rm FEL}(s)$ satisfies the passivity. Thus, the learning of $\hat{P}^{-1}(s)s$ can be stabilized.

In the PFC, the augmented error $(e - \theta_{\rm PFC})$ rather than e in (4) converges to zero using the NN for stabilization of learning of $\hat{P}^{-1}(s)s$. Thus, e in (4) does not necessarily converge to zero in steady state. In most cases, an offset remains, i.e., $\theta_{\rm re} \neq \theta^*_{\rm re}$. To reduce the offset, K in (7) must be small.

3.2 NN for $\boldsymbol{u_{\rm FF}}$ Although differentiating operation is not needed in the proposed position control system, the input to the ACR may still become excessive due to load. Therefore, a saturator is required for system protection regardless of the structure of the position control system. In the proposed position control system, the FF controller is trained by the NN to estimate $s\hat{P}^{-1}(s)$ even when the nonlinearity caused by the saturator exists.

Fig. 4 shows the structure of the NN to generate $u_{\rm FF}$ in Fig. 3. The NN is composed of three independent sub-NNs. Each sub-NN is composed of one input, two hidden, and one output layers. Each hidden layer has three nodes. Let $n_{m,l,k}$ denote the m-th ($m = 1$ for $l = 1, 4$ and $m = 1, 2, 3$ for $l = 2, 3$) node in the l-th ($l = 1, 2, 3, 4$) layer of the k-th ($k = 1, 2, 3$) sub-NN. In Fig. 4, $H_{m,l,k}$, $F_{m,l,k}$, $w_{m,l,k}$, and $b_{m,l,k}$ ($m = 1$ for $l = 1$ and $m = 1, 2, 3$ for $l = 2, 3$), ($l = 1, 2, 3$), ($k = 1, 2, 3$) denote the input, activate function, weighting vector, and bias vector of $n_{m,l,k}$, respectively. $F_{m,l,k}$ for all m, l, and k is $\tanh(\cdot)$. Since the reference trajectories $\theta^*_{\rm re}$ is given in advance, $\dot{\theta}^*_{\rm re}$, $\ddot{\theta}^*_{\rm re}$, and $\dddot{\theta}^*_{\rm re}$, are available. Each input to the corresponding sub-NN is normalized as $\frac{\dot{\theta}^*_{\rm re}}{\max(|\dot{\theta}^*_{\rm re}|)}$, $\frac{\ddot{\theta}^*_{\rm re}}{\max(|\ddot{\theta}^*_{\rm re}|)}$, and $\frac{\dddot{\theta}^*_{\rm re}}{\max(|\dddot{\theta}^*_{\rm re}|)}$ so that it is within $[-1, 1]$.

Each sub-NN outputs ${}^k u_{\rm FF}$ ($k = 1, 2, 3$). Thus, the NN generates $u_{\rm FF}$ as the sum of ${}^k u_{\rm FF}$ ($k = 1, 2, 3$). The general backpropagation (BP) algorithm is used to update $w_{m,l,k}$ and $b_{m,l,k}$ ($m = 1$ for $l = 1$ and $m = 1, 2, 3$ for $l = 2, 3$), ($l = 1, 2, 3$), ($k = 1, 2, 3$) in the NN.

4. Experiment

This section shows the effectiveness of the proposed position controller by comparing it with the conventional controller [7]. In particular, e in (4) is evaluated to see the influence of the torque disturbance against the estimation performance of $\hat{\boldsymbol{\alpha}}$ or $u_{\rm FF}$ and $\hat{\theta}_{\rm re}$.

4.1 Experimental condition Table 2 lists the nominal parameters of the test IPMSMs. All calculation is executed in DSP (Myway Plus Corporation: Expert IV). The carrier frequency of the three-phase voltage-

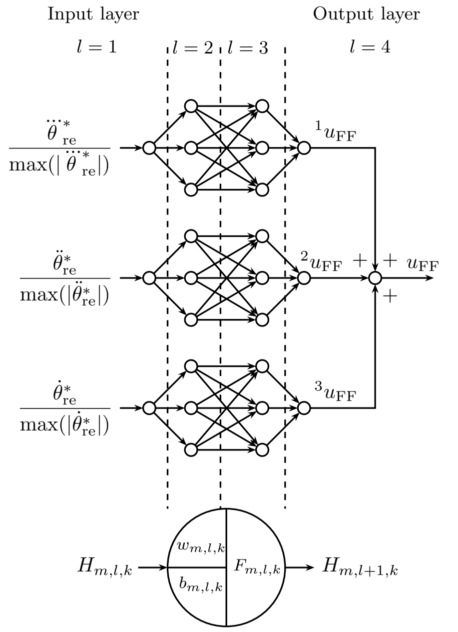

$H_{m,l+1,k} = F_{m,l,k}(w_{m,l,k}\ H_{m,l,k} + b_{m,l,k})$

($m = 1$ for $l = 1, 4$ and $m = 1, 2, 3$ for $l = 2, 3$), ($l = 1, 2, 3$), ($k = 1, 2, 3$)

Fig. 4. Structure of NN.

Table 2. Parameters of test IPMSMs.

Parameters	IPMSM#1	IPMSM#2
J_n	0.0081 kgm^2	0.76 kgm^2
R	0.681 Ω	1.10 Ω
L_d	10.0 mH	10.4 mH
L_q	15.2 mH	12.4 mH
K_e	0.375 Vs	0.214 Vs
P_n	3	4
Rated power	1.5 kW	1.0 kW
Rated speed	1450 min^{-1}	2000 min^{-1}
Rated line voltage	174 V	200 V
Rated line current	5.7 A	6.4 A

type pulse-width modulation (PWM) inverter is 10 kHz. The control period synchronized with the triangle-wave PWM carrier is $T_s = 100\ \mu$s. All controllers and learning are synchronized with the triangular-wave PWM carrier. The cut-off frequencies of the ACR and the APR shown in Fig. 1 are 2000 rad/s and 5.0 rad/s, respectively.

To generate θ^*_{re} in the positioning control, the following function is used:

$$r(t) = 6t^5 - 15t^4 + 10t^3. \qquad (10)$$

Note that $\dot{r}(t) = 0$ at $t = 0$, 1. For the given target angle L and the moving time T, we define $\theta^0_{\mathrm{re}}(t)$ $(0 \le t < 4T)$ as follows:

$$\theta^0_{\mathrm{re}}(t; L, T) = \begin{cases} Lr\left(\dfrac{t}{T}\right) & (0 \le t < T), \\ L & (T \le t < 2T), \\ Lr\left(-\dfrac{t-3T}{T}\right) & (2T \le t < 3T), \\ 0 & (3T \le t < 4T). \end{cases} \qquad (11)$$

Using (11), we set $\theta^*_{\mathrm{re}}(t)$ as the following periodic position reference:

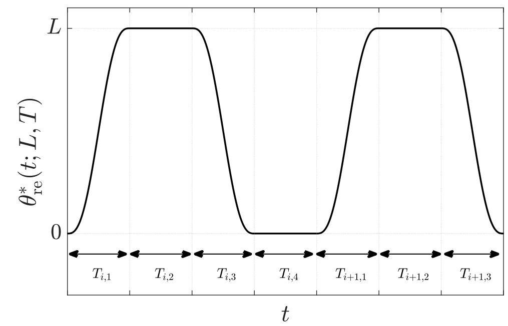

Fig. 5. $\theta^*_{\mathrm{re}}(t; L, T)$ in (12).

$$\theta^*_{\mathrm{re}}(t; L, T) = \theta^0_{\mathrm{re}}(t - t_i; L, T) \quad (t_i \le t < t_{i+1}) \qquad (12)$$

where $t_i = 4(i-1)T$ $(i = 1, 2, \ldots)$. For convenience, we define $T_{i,j} = [t_i + (j-1)T,\ t_i + jT)$ $(i = 1, 2, \ldots)$ and $(j = 1,\ 2,\ 3,\ 4)$. Fig. 5 shows $\theta^*_{\mathrm{re}}(t; L, T)$ in (12) and $T_{i,j}$ $(i = 1, 2, \ldots)$ and $(j = 1,\ 2,\ 3,\ 4)$. In Fig. 5, $T_{i,1}$ and $T_{i,3}$ $(i = 1, 2, \ldots)$ correspond to transient state while $T_{i,2}$ and $T_{i,4}$ correspond to steady state.

In the experiments, we set $L = 30$ deg in electrical angle (10 deg in mechanical angle) and $T = 250$ ms (for IPMSM#1) and 1.0 s (for IPMSM#2). In the proposed method, $\dot{\theta}^*(t)$, $\ddot{\theta}^*_{\mathrm{re}}(t)$ and $\dddot{\theta}^*_{\mathrm{re}}(t)$ are given as the first, second, and third differential of $\theta^*_{\mathrm{re}}(t)$, respectively.

To evaluate the proposed method, we define

$$\hat{e} := \hat{\theta}_{\mathrm{re}} - \theta_{\mathrm{re}}. \qquad (13)$$

In the experiments, due to digital control $e[k] = e(kT_s)$ and $\hat{e}[k] = \hat{e}(kT_s)$ where k $(k = 0, 1, \ldots)$ is the sampling step.

The tracking error in transient state is evaluated by the following criterion:

$$J_{\mathrm{tets}} := \max_{kT_s \in T_{i,1} \cup_i T_{i,3} \cdots} |e[k]|. \qquad (14)$$

The estimation error is evaluated by the following criterion:

$$J_{\mathrm{ee}} := \max_k |\hat{e}[k]|. \qquad (15)$$

4.2 Results for no load Fig. 6 shows the experimental results of positioning control with (a) the conventional and (b) the proposed methods for IPMSM#1 without load. From Fig. 6, it can be observed that $\hat{e}$ in transient state by the conventional method is larger than that by the proposed method. By contrast, $\hat{e}$ in steady state by the two methods is similar. In the conventional method, $\hat{e}$ in transient state is mainly caused by the differential calculation of $\hat{\boldsymbol{\alpha}}$.

Table 3 evaluates the results shown in Fig. 6 quantitatively. From Table 3, we can see that both J_{tets} (tracking error in transient state) and J_{ee} (estimation error) by the proposed method are less than those by the conventional method, which validates the effectiveness of the proposed method. In the proposed method, $\hat{\boldsymbol{\alpha}}$ is learned such that $(e - \theta_{\mathrm{PFC}})$ is zero. In other words, $e = \theta_{\mathrm{PFC}}$ holds instead of $e = 0$. Therefore, an offset in

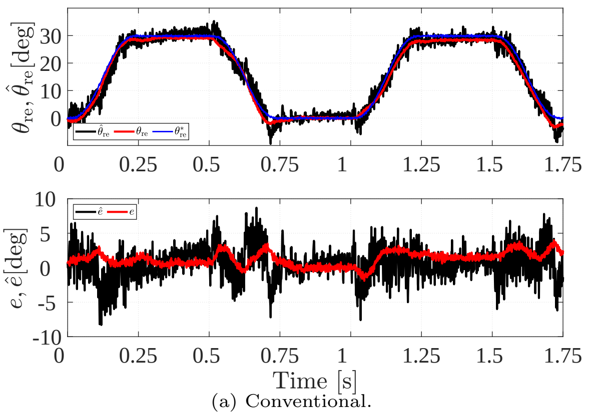

(a) Conventional.

(b) Proposed.

Fig. 6. Positioning control results w/o load.

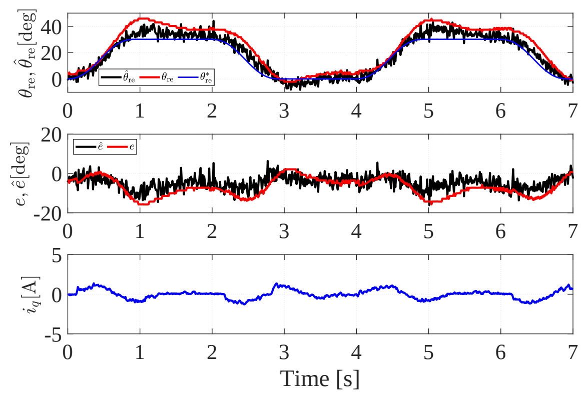

(a) Conventional.

(b) Proposed.

Fig. 7. Experimental results of positioning control (IPMSM#2 coupled to inertia load).

Table 3. Evaluation of experimental results for no load shown in Fig. 6.

Criterion	(a) con.	(b) pro.
$J_{\rm tets}$ (tracking error in transient state)[deg]	4.0	3.3
$J_{\rm ee}$ (estimation error)[deg]	8.7	6.0

Table 4. Evaluation of experimental results for load shown in Fig. 7.

Criterion	(a) con.	(b) pro.
$J_{\rm tets}$ (tracking error in transient state)[deg]	14.0	10.2
$J_{\rm ee}$ (estimation error)[deg]	16.1	13.7

the position control result due to the $\theta_{\rm PFC}$ is essentially unavoidable. Nevertheless, the slight drawback of the PFC is not an issue since $J_{\rm tets}$ and $J_{\rm re}$ is lower than that by the conventional method.

From the experimental results, we can conclude that the proposed method is more effective than the conventional method from the tracking control performance in no-load conditions.

4.3 Results for inertia load Load tests are conducted to verify the effectiveness of the proposed method. In the experiment, IPMSM#2 is coupled to an inertia load for more practical use.

Fig. 7 shows the experimental results of positioning control with (a) the conventional and (b) the proposed methods. From Fig. 7, we can observe that both two methods achieve positioning control without destabilization.

Table 4 evaluates the experimental results shown in Fig. 7. From Table 4, all criteria $J_{\rm tets}$, and $J_{\rm ee}$ by the proposed method are smaller than those by the conventional method, which validates the proposed method is more effective than the conventional method even if an inertia load exists.

The position estimation error of IPMSM#2 is larger than that of IPMSM#1 due to the small saliency of IPMSM#2 since the saliency of the IPMSM is used in the proposed method. Therefore, the position control error of IPMSM#2 is larger than that of IPMSM#1 as shown in Fig. 6 and Fig. 7. Nevertheless, the position control error in mechanical degree is almost same for IPMSM#1 and IPMSM#2.

4.4 Results for inertia load fluctuation We further show the proposed method is effective even for load fluctuation. We apply the proposed method to IPMSM#1. In this experiment, the coupled inertia load fluctuates, which is simulated by using a load motor as

$$\tau_l = \frac{1}{1+\Delta}\tau_m, \tag{16}$$

where τ_l and Δ denote the load torque and inertia fluctuation ratio, respectively, and †

$$\tau_m = P_n(K_e + (L_d - L_q)i_d)i_q. \tag{17}$$

In the experiments, $\Delta = 1.0$, 3.0, and 5.0 in (16) are tested.

† In (17), i_d and i_q are calculated using $\theta_{\rm re}$ from the encoder that is used only for the load motor torque control, but is not used for positioning control. (see Appendix for the detail).

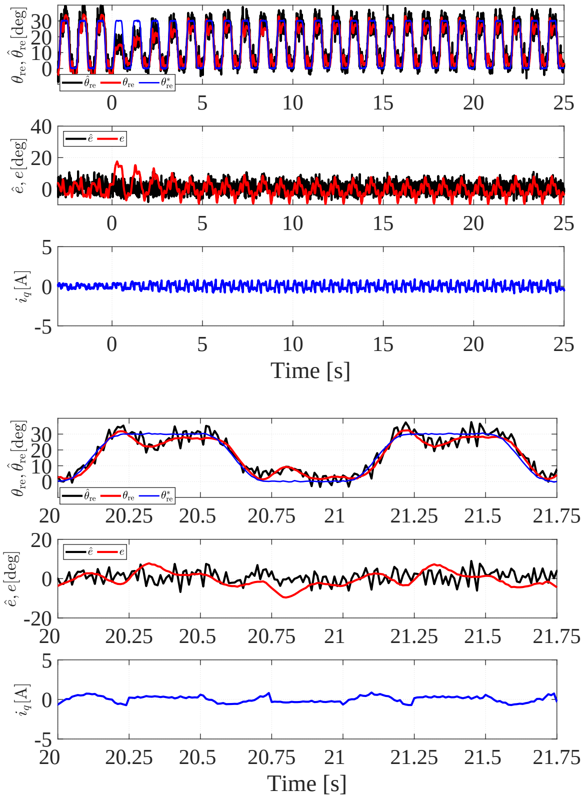

Fig. 8. Experimental result of conventional method with load ($\Delta = 1.0$ (bottom: enlarged plot from 20s to 21.75s)).

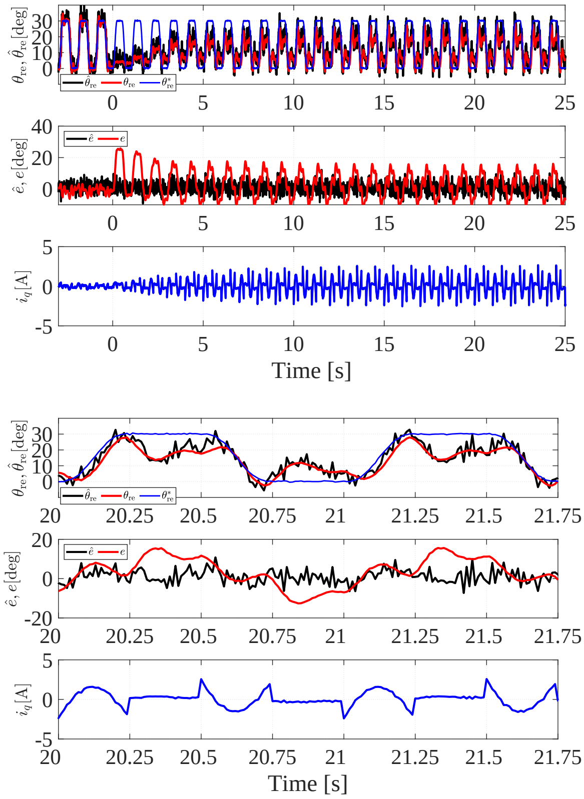

Fig. 9. Experimental result of conventional method with load ($\Delta = 3.0$ (bottom: enlarged plot from 20s to 21.75s)).

Figs. 8-10 and 11-13 show the experimental results of $\Delta = 1.0$, 3.0, and 5.0 with the conventional and proposed methods, respectively. From Fig. 10, it can be observed that the conventional method becomes unstable when $\Delta = 5.0$, resulting that $\theta_{\rm re}$ diverges. The estimation of $\hat{\boldsymbol{\alpha}}$ in the conventional method is not robust since the load fluctuation is equivalently compensated by adjusting $\hat{\boldsymbol{\alpha}}$ in (5). The estimation of $\hat{\boldsymbol{\alpha}}$ using (5) is much slower than the load fluctuation, and thus, the estimation error of $\hat{\boldsymbol{\alpha}}$ leads to loss synchronism. By contrast, from Figs. 11-13, we can observe that the proposed method achieves positioning control without destabilization in all cases successfully. Since $\hat{\boldsymbol{\alpha}}$ are learned in the NN of the proposed method, $\hat{\boldsymbol{\alpha}}$ is always available even if $\hat{\boldsymbol{\alpha}}$ is not linear with respect to i_q regardless of load fluctuation.

Table 5 evaluates the experimental results shown in Figs. 8-10 and 11-13. From Table 4, all criteria $J_{\rm tets}$, and $J_{\rm ee}$ by the proposed method are superior to those of the conventional method, which demonstrates that the proposed method is more effective than the conventional method, even with an inertia load fluctuation.

These experimental results validate the effectiveness of the proposed position-sensorless positioning servo system.

4.5 Results for $\boldsymbol{u_{\rm FF}}$ and $\boldsymbol{u_{\rm FB}}$ We finally show the relationship between $u_{\rm FF}$ and $u_{\rm FB}$ in the proposed method. We apply the proposed method IPMSM#1 and IPMSM#2. The experimental conditions are the same as with Sections 4.3 and 4.4.

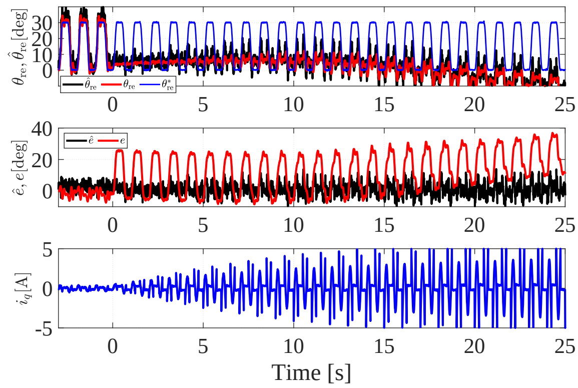

Fig. 10. Experimental result of conventional method with load ($\Delta = 5.0$ (no enlarged plot)).

Table 5. Evaluation of experimental results shown in Figs. 8-9 and 11-10.

	con.			pro.		
Criterion	$\Delta = 1.0$	$\Delta = 3.0$	$\Delta = 5.0$	$\Delta = 1.0$	$\Delta = 3.0$	$\Delta = 5.0$
$J_{\rm tets}$[deg]	9.2	16.7	–	7.1	6.5	6.9
$J_{\rm ee}$[deg]	5.5	8.8	–	2.9	4.0	5.3

Fig. 14 shows the relationship between $u_{\rm FF}$ and $u_{\rm FB}$ for IPMSM#2. In the standstill, $u_{\rm FB}$ is not zero since the learning of $\hat{\boldsymbol{\alpha}}$ stops as $\boldsymbol{\xi}$ equals zero. By contrast, $u_{\rm FB}$ is almost zero during moving,, indicating that i_q^* is mainly generated from $u_{\rm FF}$ after the completion of

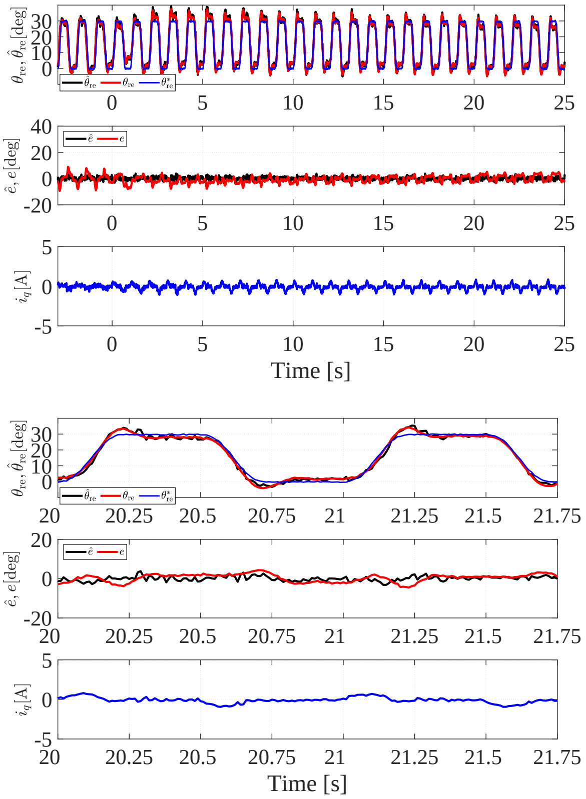

Fig. 11. Experimental result with proposed method with load ($\Delta = 1.0$ (bottom: enlarged plot from 20s to 21.75s).

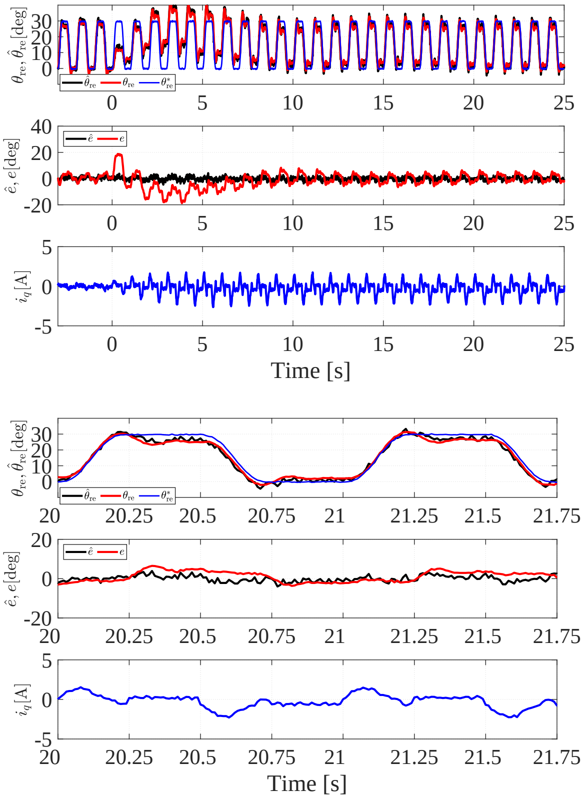

Fig. 12. Experimental result with proposed method with load ($\Delta = 3.0$ (bottom: enlarged plot from 20s to 21.75s)).

learning.

Fig. 15 shows the relationship between u_{FF} and u_{FB} for IPMSM#1 when $\Delta = 1.0$. Note that the relationship between u_{FF} and u_{FB} does not depend on Δ. From the top plot of Fig. 15, it can be observed that u_{FF} increases after the load is applied, indicating that u_{FF} is larger than u_{FB}. From the bottom plot of Fig. 15, it can be observed that u_{FF} is more dominant than u_{FB} during moving. The results when $\Delta = 3.0$ and 5.0 are skipped since the relationship between u_{FF} and u_{FB} is similar to the case when $\Delta = 1.0$.

This result validates that the proposed learning method is effective even when a load is applied.

5. Conclusion

This paper proposed a novel FEL-based position control system in the position-sensorless positioning servo systems. In the proposed method, the FF controller established via learning compensated the parameter fluctuations adaptively in the systems. As the learning progressed, the output of the FEL controller became dominant than the FB controller. Thus, the transient response of the position control was improved. Since the FB controller continued to operate even after completion of the learning, robustness to the disturbance torque was guaranteed.

Future works include the improving the accuracy and response of the position estimation furthermore.

References

(1) O. C. Ferreira and R. Kennel, “Encoderless Control of Industrial Servo Drives,” in *Proc. of 12th International Power Electronics and Motion Control Conference*, pp. 1962–1967, Portoroz, Slovenia, Sep. 2009.

(2) F. Cupertino, G. Pellegrino, P. Giangrande, and L. Salvatore, “Sensorless Position Control of Permanent-Magnet Motors With Pulsating Current Injection and Compensation of Motor End Effects,” *IEEE Trans. Ind. Appl.*, vol. 47, no. 3, pp. 1371–1379, Mar. 2011.

(3) S. Sato and K. Ide, “Application Trends of Sensorless AC Motor Drives in Europe,” *IEEJ journal of Ind. Appl.*, vol. 3, no. 2, pp. 97–103, Apr. 2014.

(4) O. Ni, M. Yang, S. A. Odhano, P. Zanchetta, X. Liu, and D. Xu, “Analysis and Design of Position and Velocity Estimation Scheme for PM Servo Motor Drive with Binary Hall Sensors,” in *2018 IEEE Energy Conversion Congress and Exposition (ECCE)*, pp. 6967–6974, Portland, OR, USA, Sep. 2018.

(5) M. O. M. Kakihara, M. Takaki and S. Morimoto, “Investigation of Servomotor Structure for Sensorless Control Based on High-Frequency Injection Method,” *IEEJ Journal of Ind. Appl.*, vol. 10, no. 6, pp. 718–725, Nov. 2021.

(6) N. Kawamura, M. Hasegawa, K. Z. Liu, and T. Zanma, “Position-sensorless adaptive positioning control system for ipmsms,” *IET Electric Power Applications*, vol. 13, no. 2, pp. 138–146, Nov. 2019.

(7) N. Kawamura, T. Zanma, K. Koiwa, K.-Z. Liu, and M. Hasegawa, “Position Sensorless Adaptive Positioning Servo System with Simplified Differential Calculation and High-Frequency Voltage Injection Strategy Considering Acoustic Noise Suppression,” *IEEJ Journal of Industry Applications*, vol. 10, no. 1, pp. 1–10, Jan. 2021.

(8) M. Kawato, K. Furukawa, and R. Suzuki, “A hierarchical neural-network model for control and learning of voluntary

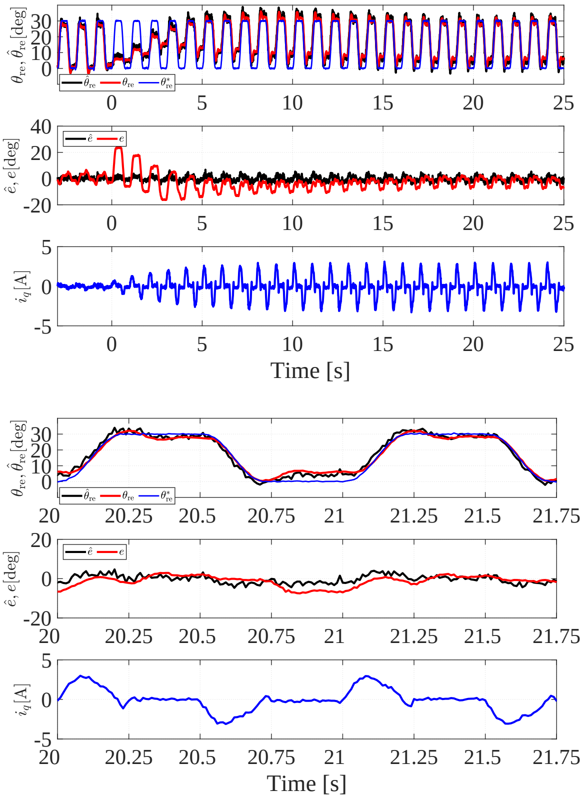

Fig. 13. Experimental result with proposed method with load ($\Delta = 5.0$ (bottom: enlarged plot from 20s to 21.75s)).

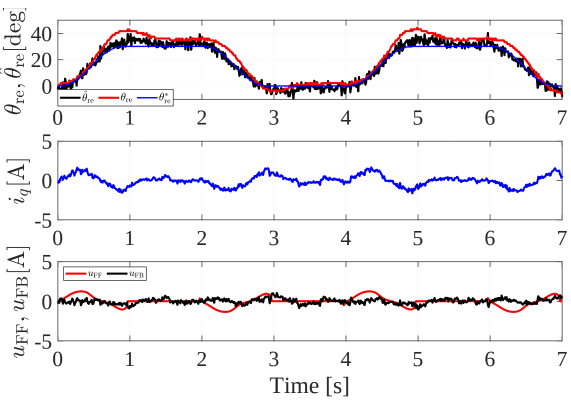

Fig. 14. Relationship between u_{FF} and u_{FB} (IPMSM#2 coupled to inertia load).

movements," *Biological. Cybernetics*, vol. 57, no. 3, pp. 169–185, Oct. 1987.

(9) A. Miyamura and H. Kimura, "Stability of feedback error learning scheme," *Systems Control Letters*, vol. 45, no. 4, pp. 303–316, Dec. 2002.

(10) E. Muramatsu and K. Watanabe, "Feedback error learning control without recourse to positive realness," *IEEE Transactions on Automatic Control*, vol. 49, no. 10, pp. 1762–1770, Oct. 2004.

(11) B. Phokaphan, P. Guptabutra, T. Onwan, S. Wongsura, and W. Kongprawechnon, "Theoretical Discussion on the Discrete-Time Feedback Error Learning for a Time Delay System with an Uncertainty Plant Model by using a PD Controller," in *2007 Power Conversion Conference - Nagoya*, pp. 172–176, Nagoya,Japan, Apr. 2007.

(12) T. Suzuki, M. Hasegawa, M. Tomita, and S. Doki, "Initial position estimation for IPMSMs using comb filters and effects

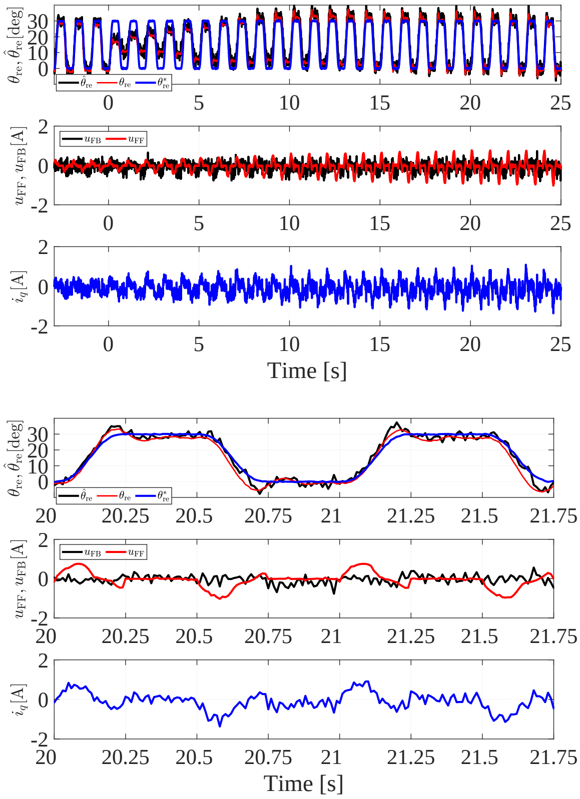

Fig. 15. Relationship between u_{FF} and u_{FB} with $\Delta = 1.0$ (bottom: enlarged plot from 20s to 21.75s).

on various injected signal frequencies," *IEEJ journal of Ind. Appl.,*, vol. 4, no. 3, pp. 204–211, May. 2015.

(13) R. Ortega, "On Morse's New Adaptive Controller: Parameter Convergence and Transient Performance," *IEEE Trans. Autom. Control*, vol. 47, no. 3, pp. 1191–1202, Aug. 1993.

(14) K. J. Astrom and B. Wittenmark, *Adaptive control*, 2nd ed. MA, USA: Addison Wesley.

(15) P. A. Ioannou and J. Sun, *Robust adaptive control.* Upper Saddle River, NJ, USA: Prentice-Hall International, Inc., 1996.

(16) S. Fujii and I. Mizumoto, "Design of Discrete Time Output Feedback Control System with Adaptive Parallel Feedforward Compensator," in *2018 Australian & New Zealand Control Conference (ANZCC)*, pp. 75–80, Melbourne, VIC, Australia, Dec. 2018.

Appendix

1. Derivation of relationship between u_{FB} and $(\hat{P}^{-1}(s)s - P^{-1}(s)s)$

We derive the relationship between u_{FB} and $(\hat{P}^{-1}(s)s - P^{-1}(s)s)$ for stability analysis of the learning of $\hat{P}^{-1}(s)s$ by passivity, From (2),

$$\begin{aligned} e &= \theta^*_{\mathrm{re}} - \theta_{\mathrm{re}} \\ &= s^{-1}P(s)u_0 - s^{-1}P(s)(u_{\mathrm{FF}} + (K_P + sK_D)e) \end{aligned} \tag{A1}$$

From (A1), we obtain

$$\begin{aligned} e &= \frac{-s^{-1}P(s)}{1 + s^{-1}P(s)(K_P + sK_D)}(u_{\mathrm{FF}} - u_0) \\ &= \frac{-s^{-1}P(s)}{1 + s^{-1}P(s)(K_P + sK_D)}(\hat{P}^{-1}(s)s - P^{-1}(s)s)\theta^*_{\mathrm{re}}. \end{aligned} \tag{A2}$$

In Fig. 3, e can also be written as

$$e = (K_P + sK_D)^{-1} u_{\mathrm{FB}}. \tag{A3}$$

From (A2) and (A3), the relationship between u_{FB} and $(\hat{P}^{-1}(s)s - P^{-1}(s)s)$ can be given as:

$$u_{\mathrm{FB}} = \frac{-s^{-1}P(s)(K_P + sK_D)}{1 + s^{-1}P(s)(K_P + sK_D)} (\hat{P}^{-1}(s)s - P^{-1}(s)) s\theta^*_{\mathrm{re}}. \tag{A4}$$

Applying the $C_{\mathrm{PFC}}(s)$, we replace $s^{-1}P(s)$ with $\tilde{G}(s)$ yields (9).

2. Derivation of an inertia load fluctuation simulated by using the load motor

For simulating the inertia load fluctuation, we derive the relationship between an inertia fluctuation and a torque fluctuation due to the fluctuation. Assuming that there is no inertia fluctuation and constant rotor speed, the equation of motion for IPMSM can be given by

$$\omega_{\mathrm{rm}} = \frac{1}{J_n s} \tau_m. \tag{A5}$$

Considering the fluctuations of J_n and ω_{rm} in (A5), we obtain

$$\delta\omega_{\mathrm{rm}} + \omega_{\mathrm{rm}} = \frac{1}{(J_n + \delta J)s} \tau_m. \tag{A6}$$

From (A5) and (A6), we obtain the following relationship:

$$\delta\omega_{\mathrm{rm}} = \frac{1}{(J_n + \delta J)s} \tau_m - \frac{1}{J_n s} \tau_m. \tag{A7}$$

From (A7), we obtain

$$\begin{aligned} \delta\omega_{\mathrm{rm}} &= \frac{1}{(J_n + \delta J)s} \tau_m - \frac{1}{J_n s} \tau_m \\ &= \frac{-\delta J}{J_n (J_n + \delta J)s} \tau_m \\ &= -\frac{1}{J_n s} \left(1 - \frac{J_n}{(J_n + \delta J)}\right) \tau_m \\ -\delta\omega_{\mathrm{rm}} &= \frac{1}{J_n s} \tau_m - \frac{1}{J_n s} \frac{J_n}{(J_n + \delta J)} \tau_m \\ &= \frac{1}{J_n s} \tau_m - \frac{1}{J_n s} \underbrace{\frac{1}{(1+\Delta)} \tau_m}_{=:\tau_l}, \end{aligned} \tag{A8}$$

where $\Delta = \frac{\delta J}{J_n}$ is the inertia fluctuation ratio. From (A8), the inertia fluctuation is simulated by applying the τ_l from the load motor to the test IPMSM. From the above, we obtain (16).

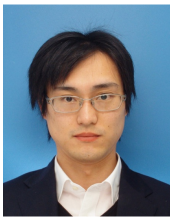

Naoki Kawmaura (Member) was born in 1993. He received the B.Eng., and M.Eng., degrees from Chubu University, Japan, in 2016 and 2018, respectively, and the Ph.D. degree from Chiba University, Japan, in 2021, all in electrical engineering. In 2021, he joined the NEXT JAPAN CORPORATION. Since 2021, he has been with Dept. of Systems and Design Eng., Seikei University, Japan, as an Assistant Professor, visiting researcher in Chubu University, and adjunct researcher in Waseda University. His current research interests are adaptive/learning control theory, power electronics, motion control, motor drive and their applications. He is a member of IEEE and SICE.

Shota Inoue (Non-member) was born in 1997. He received the B. Eng., M. Eng. degrees in electrical engineering from Chiba University, Chiba, Japan, in 2020 and 2022, respectively. His research interest is position sensorless contorl.

Tadanao Zanma (Senior Member) was born in 1972. He received the B. Eng., M. Eng., and Ph. D from Nagoya University in 1995, 1997 and 2000, respectively, all in Electrical Engineering. From 2000 to 2007, he was with Mie University initially as a Research Associate, and since 2007, as an Assistant Professor. In 2007, he was an academic guest in ETH Zurich. He was an Associate Professor at Mie University from 2009 to 2011. He has been with Chiba University as an Associate Professor since 2011. His current research interests include hybrid dynamical control, switched systems, networked control systems, especially system control based on mixed logical dynamical systems and model predictive control. He has received FANUC FA and Robot Foundation thesis prize in 2009, and IEEJ Distinguished Paper Award 2010 and 2015. He is a member of SICE, ISCIE, and IEEE.

Keiichiro Kondo (Senior Member) received B.S. and Dr. Eng. from Faculty of Electrical Engineering, Department of Science and Technology, Waseda University in 1991 and 2000, respectively. He was with Railway Technical Research Institute from 1991 to 2006 and had been engaged at R&D for power electronics applied railway vehicle traction system. From 2007 to 2018, he was with Electrical and Electronic Engineering Course of Graduate School of Chiba University. Since 2018, he has been with School of Advance Science and Engineering, Department of Electrical Engineering and Bio Science, Waseda University as a professor. His current research interests are power electronics, AC motor drive, energy storage devices, wireless power transmission and their applications to the railway system. Prof. Kondo titled Professional Engineer in Japan (Mechanical Engineering, TechnicalManagement). He is a Senior Member of the Institute of Electrical Engineers of Japan (IEEJ) and a Member of IEEE.

Kenta Koiwa (Member) was born in 1989. He received the B. E. and M. E. degrees in electrical engineering from the Kitami Institute of Technology, Japan, in 2012 and 2014, respectively, and the Ph. D. degree in electrical engineering from Chiba University, Japan, in 2017, where he has been an Assistant Professor with the Department of Electrical and Electronic Engineering. His research interests include power systems, renewable energy, and power electronics. He is a member of IEEE.

Kang-Zhi Liu (Member) was born in 1964. He received the B. E. degree from North-Western Polytechnical University, Xi'an, China, in 1984, the M. E. and Ph. D degrees from Chiba University, Chiba, Japan, in 1988 and 1991, respectively. Then, he joined Chiba University and is now a Professor. He has authored six books. His main fields are control theory, power system, smart grid, and electrical drives. Prof. Liu was a recipient of the Young Author Award and the three Best Paper Awards from SICE, Japan. He was the Director of SICE from 2017 to 2018.

Masaaki Shibata (Senior Member) was born in 1968. He received B.E., M.E. and Ph.D. degrees in Electrical Engineering from KEIO University, in 1991, 1993 and 1996, respectively. Since 1998, he has been with SEIKEI University, in Tokyo, JAPAN. From 2010, he has been a Professor in SEIKEI University. His research interests include "Robotic", "Visual Servoing" and "Object Recognition with Image Processing".